Systematic analysis of semiconductor photoconductivity dynamics under different laser excitations: two- and three-level models

fatima zohra Mahi (fati_zo_mahi2002@yahoo.fr)
Exacte Sciences
Abdelhamid Mahi
Sciences and advanced materials laboratory
Fatima Zohra Mahi
Exacte Sciences of Algeria university
Alaeddine Abbes
INRS: Institut national de la recherche scientifique
Luca Varani
Institut d'Electronique et des Systemes

Research Article

Keywords: Photoconductivity, pulse laser, continuous-wave laser, generation and recombination rates, partial differential equations

Posted Date: July 19th, 2022

DOI: https://doi.org/10.21203/rs.3.rs-1797627/v1

Systematic analysis of semiconductor photoconductivity dynamics under different laser excitations: two- and three-level models

Abdelhamid Mahi[1], Fatima Zohra Mahi[2], Alaeddine Abbes[3,4], Christophe Palermo[3] and Luca Varani[3]

[1]Institute of Sciences, Instrumentation and Advanced Materials Laboratory, Nour Bashir University Center of El Bayadh, Algeria.
[2]Faculty of Exact Sciences, Department of Materials Sciences, Tahri Mohammed University of Bechar, Algeria.
[3]IES, University of Montpellier, CNRS, Montpellier, France.
[4]Institut National de la Recherche Scientifique, Centre Énergie Matériaux Télécommunications (INRS-EMT), Varennes, Canada.

Abstract

A numerical study of a model photoconductor under pulse and continuous-wave laser excitation is presented. From the solution of a system of partial differential equations related to the populations of conduction and valence bands we analyze the time behavior of the photoexcited concentrations of electrons and holes where the diffusion phenomena and the presence of electric field are neglected. Additionally, for the three-level model, the population of traps level is also introduced and analyzed as a third variable. The dynamics of electrons, holes and traps levels concentrations are studied in the presence of different types of pulse and harmonic laser photoexcitations. We show that an improved physical insight is obtained through a systematic analysis of the influence of the main physical parameters, such as generation and recombination rates, between the available energy levels.

Keywords: Photoconductivity, pulse laser, continuous-wave laser, generation and recombination rates, partial differential equations.

1 Introduction

The photoconductive phenomenon, i.e. the physical mechanism which creates electron-hole pairs from the absorption of electromagnetic radiation, thus changing the electrical conductivity, has been extensively studied for its interest in fundamental material properties and for several practical applications [1]. Depending on the specific material, the transitions of electrons and holes take place either directly between valence band (VB) and conduction band (CB) or through trap levels (TL) situated in the energy gap. A careful analysis of the dynamics of these transitions is necessary for the optimization of different radiations detectors, photoconductive switches and other photoelectric devices [2, 3].

As a recent example, semiconductor-based photoconductors are more and more studied for high-frequency generation of electromagnetic

waves with rapid progress over the past decade [4, 5]. In this context, high-speed photodiodes, e.g. Uni-Traveling Carrier photodiodes [6, 7], are emerging as essential devices for high data-rate communication and related methods such as beam-steering [8, 9, 10, 11]. Indeed, the photoconductive-based sources are considered as promising emitting devices because they can be coherent, widely tuneable and cost-effective by operating at room-temperature [12, 13, 14, 15].

While the generation of short pulses using optical excitation from ultrafast lasers has been studied in the literature [16], the case of continuous-wave (CW) generation by downconverting two single-mode laser signals or a dual-mode laser signal has received less attention [14] even if such an analysis is mandatory to model correctly photomixer sources [10, 17, 18]. Moreover, even in the case of pulsed excitations, available studies are usually limited to a specific situation using a single set of physical parameters.

To fill this lack of knowledge, in this paper, we propose a simple but systematic numerical analysis of the physical processes that take place in a model semiconductor material excited by pulse (Gaussian and square temporal functions) and CW harmonic laser signals. The physical model is based on a system of coupled differential equations describing the band-to-band generation and recombination processes possibly coupled to the release and capture rates associated with the transitions between the TL and the bands. In particular, we present two models both taking into account different excitation scenarios of interest for practical situations. The former one is a two-level model which considers only the transitions between the VB and the CB for different pulse durations and harmonic frequencies of laser excitation. The latter one is a more complex three-level model which includes the presence of TL between the VB and the CB. In this case we analyze the effect of changing the release and capture rates as well as the characteristic times and frequencies of the laser excitations.

2 Physical model

This section describes the physical model used to study the photoconductive dynamics of a model semiconductor bulk sample excited by a laser emitting photons at wavelength λ (and frequency ν) and producing electron-hole pairs. The spatio-temporal dynamics of the photo-excited electrons and holes can be modeled by a system of coupled equations describing the evolution of the photoexcited electron $n(t)$ and hole $p(t)$ concentrations, within the CB and VB respectively, as functions of time t. By assuming a negligible electric field and neglecting diffusion phenomena, one can consider that the carrier population and dynamics are only affected by the generation-recombination (GR) processes:

$$\frac{dn(t)}{dt} = G_n - R_n \tag{1}$$

and

$$\frac{dp(t)}{dt} = G_p - R_p, \tag{2}$$

where, for electrons and holes respectively,

- G_n and G_p are the generated densities of carriers per unit time ;
- R_n and R_p are the recombinated densities of carriers per unit time.

For most of semiconductor materials, it has been shown that an important role can be played by traps whose energy levels are located within the energy gap [1]. Such traps can be intrinsically present as defects in the semiconductor bulk material or intentionally introduced in order to decrease substantially the carriers lifetimes for high-frequency applications [20, 21, 19]. These levels can be occupied by electrons and/or holes, depending on their positions within the band gap. In this work, we consider the case of a single level trapping both electrons and holes. We assume that the traps are distributed in a homogeneous way in the semiconductor with a density sufficiently low to be represented by a single TL. Since the TL concerns both electron and holes, we describe the trap population through the trapped electron density only $n_t(t)$, and we note N_t the available electron states density, so that the trapped hole density at time t is equal to $N_t - n_t(t)$. In these conditions, the trap electron population n_t depends only on the generation-recombination processes, so that

$$\frac{dn_t(t)}{dt} = G_t - R_t, \tag{3}$$

where G_t and R_t are the generated and recombinated density of trapped electrons per unit time.

The generation-recombination processes associated with eqs. (1)-(3) are schematically depicted in Figs. 1 to 3 showing the possible transitions of photoexcited carriers among the VB, the CB and the TL. Electrons and holes are indicated respectively with circles and squares. The transitions between energy levels are reported as vertical arrows, and the involved carriers leave an empty symbol to reach a closed one. We can remark that, for each population, there are two generation and two recombination processes.

2.1 Generation-Recombination processes

We discuss separately the balance equations for the three variables $n(t)$, $p(t)$ and $n_t(t)$ describing respectively the CB, VB and traps levels populations. In order to make explicit the GR terms of eqs. (1)-(3), we consider that each transition induces a variation of the density equal to the product between (i) the associated transition rate, (ii) the density of carriers of the initial state (that is able to make the transition) and (iii) the available density of final states.

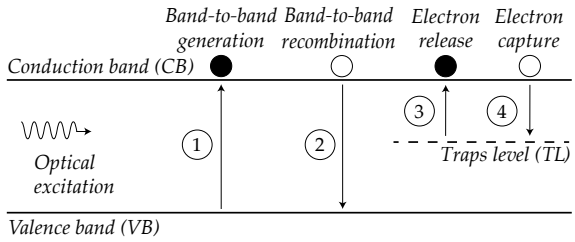

Fig. 1: Generation-recombination processes involving the electron density $n(t)$. The processes from 1 to 4 correspond to band-to-band electron generation (from VB to CB), band-to-band electron recombination (from CB to VB), electron release (from TL to CB) and electron capture (from CB to TL), respectively. Closed circles represent final occupied electron states and open circles final empty electron states, respectively.

For what concerns $n(t)$, we consider the following GR processes, ordered with the numbers corresponding to those of Fig. 1 :

1. the band-to-band generation rate. If we note N and P the densities of states of the CB and VB, respectively, and E_{vc} the transition rate in $\mathrm{cm^3 s^{-1}}$, the time variation of $n(t)$ due to this process can be written as

$$G_{n_1} = E_{vc}\ (N-n)\ (P-p), \tag{4}$$

2. the band-to-band recombination with a rate E_{cv} expressed in $\mathrm{cm^3 s^{-1}}$, so that

$$R_{n_1} = E_{cv}\ n\ p, \tag{5}$$

3. the electron release from TL to CB, which constitues a second generation term. It involves the density of trapped electrons n_t and of available CB states $N-n$ with a transition rate E_{tc}, so that:

$$G_{n_2} = E_{tc}\ n_t\ (N-n), \tag{6}$$

4. the electron capture from CB to TL, which constitues a second recombination term, involving the density of electrons n and the density of available states in the TL, $N_t - n_t$. If we note E_{ct} the transition rate, we obtain:

$$R_{n_2} = E_{ct}\ n\ (N_t - n_t). \tag{7}$$

The PDE (1) describing the time evolution of $n(t)$ can then be explicitely written as

$$\frac{\partial n}{\partial t} = E_{vc}\ (N-n)\ (P-p) - E_{cv}\ n\ p + E_{tc}\ n_t\ (N-n) - E_{ct}\ n\ (N_t - n_t). \tag{8}$$

The GR processes associated with the hole density $p(t)$ are depicted in Fig. 2 and correspond to the following processes:

1. the band-to-band recombination with transition rate H_{vc} so that

$$R_{p_1} = H_{vc}\ p\ n, \tag{9}$$

2. the band-to-band generation with transition rate H_{cv}, depending on the density of holes in the CB and the density of available states in VB

$$G_{p_1} = H_{cv}\ (N-n)\ (P-p), \tag{10}$$

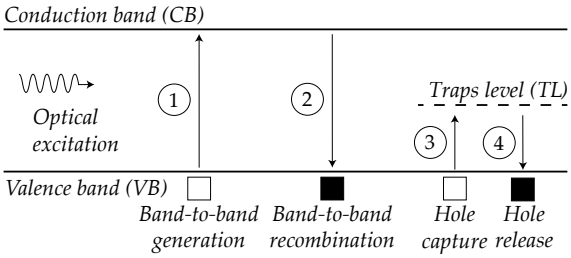

Fig. 2: Generation-recombination processes involving the hole density $p(t)$. The processes from 1 to 4 correspond to band-to-band hole recombination (from VB to CB), band-to-band hole genneration (from CB to VB), hole capture (from VB to TL) and hole release (from TL to VB), respectively. Closed squares represent final occupied hole states and open squares final empty hole states, respectively.

3. the hole capture with a transition rate H_{vt} associated with the density of holes in VB and the density of available states for holes in TL:

$$R_{p_2} = H_{vt}\ p\ n_t, \tag{11}$$

4. the hole release from TL to VB described by the transition rate H_{tv} and depending on the trapped hole population and the available VB states:

$$G_{p_2} = H_{tv}\ (N_t - n_t)\ (P - p). \tag{12}$$

Then, we obtain the following VB hole population PDE:

$$\frac{\partial p}{\partial t} = -H_{vc}\ p\ n + H_{cv}\ (N - n)\ (P - p) - H_{vt}\ p\ n_t + H_{tv}\ (N_t - n_t)\ (P - p). \tag{13}$$

Finally, the balance equation for $n_t(t)$ describes the following processes, depicted in Fig. 3 with the corresponding numbers:

- the electron release from TL to CB described with a transition rate E_{tc} through the expression

$$R_{t_1} = E_{tc}\ n_t\ (N - n), \tag{14}$$

- the electron capture from CB depending on the available electron states within the TL and on the free electron density through the transition

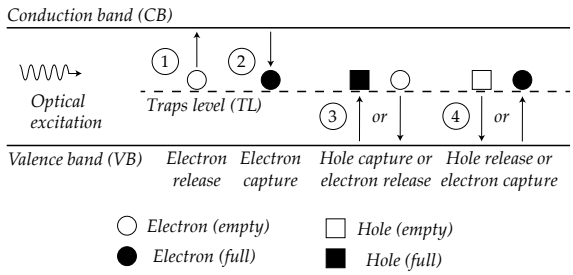

Fig. 3: Generation-recombination processes involving the trapped electrons density $n_t(t)$. The processes from 1 to 4 correspond to electron release (from TL to CB), electron capture (from CB to TL), hole capture (from VB to TL) and hole release (from TL to VB), respectively. Processes 3 and 4 can be alternatively represented as electron release (from TL to VB) and electron capture (from VB to TL), respectively Closed circles/squares represent final occupied electron/-hole states and open circles/squares final empty electron/hole states, respectively.

rate E_{ct} with the expression

$$G_{t_1} = E_{ct}\ n\ (N_t - n_t), \tag{15}$$

- the hole capture from VB to TL, that can be viewed as an electron release from TL to VB, described as

$$R_{t_2} = H_{vt}\ p\ n_t, \tag{16}$$

- the hole release from TL to VB, that can be considered as an electron trapping from VB to TL described with the transition rate H_{tv} as

$$G_{t_2} = H_{tv}\ (N_t - n_t)\ (P - p). \tag{17}$$

Therefore, we obtain the following balance equation for $n_t(t)$

$$\frac{\partial n_t}{\partial t} = -E_{tc}\ n_t\ (N - n) + E_{ct}\ n\ (N_t - n_t) + H_{tv}\ (N_t - n_t)\ (P - p) - H_{vt}\ p\ n_t. \tag{18}$$

2.2 Assumptions and simplifications

To obtain a suitable system of equations some simplifications of the equations (8), (13) and (18) can be performed.

1. As concerns the photo-generation processes, we remark that electrons and holes are always involved by pairs, so that $E_{vc} = H_{cv}$. Moreover, if we consider that the photo-generated population is negligible in comparison with the available states (that is the case of a weak photo-generation regime and a non-degenerate material), we can write that $P - p \simeq P$ and $N - n \simeq N$.

   Since N and P have constant values, the generation depends only on the transition rate, that is essentially on the power of the laser and on the photo-excited volume. Then, we can write

$$E_{vc}(N-n)(P-p) = H_{cv}(N-n)(P-p) = G, \tag{19}$$

   where G is the electron and hole photo-generation rate, given in $\mathrm{cm}^{-3}\mathrm{s}^{-1}$.
2. The photo-recombination processes also involves always holes and electrons by pairs, so that

$$E_{cv}\ n\ p = H_{vc}\ p\ n = R\ n\ p, \tag{20}$$

   where R is the photo-recombination rate given in $\mathrm{cm}^3\mathrm{s}^{-1}$.

   If we focus on the band-to-band processes, we can assume that, due to the neutrality of the material, the orders of magnitude of the quantities n and p are similar. Moreover, since we place ourselves in a regime in which the generation processes are sufficiently weak to keep the material non-degenerate, the variations of n and p can be considered sufficiently weak to suppose that $R\ n$ and $R\ p$ keep a constant value. We introduce then the band-to-band optical relaxation time τ_{bb}, so that for the cases of the electron and hole recombinations, respectively,

$$R\ n\ p = \frac{n}{\tau_{bb}} = \frac{p}{\tau_{bb}}. \tag{21}$$

3. As concerns the electron release from the trap level to the CB, the weak photo-generation regime allows to write that

$$E_{tc}\ n_t\ (N-n) = E_{tc}\ n_t\ N, \tag{22}$$

   and, since N is constant, we introduce the electron untrapping rate $g_n = E_{tc}\ N$ given in s^{-1}.
4. The same remark is made for the case of the hole untrapping, so that

$$H_{tv}\ (N_t - n_t)\ (P-p) = g_p\ (N_t - n_t), \tag{23}$$

   where $g_p = H_{tv}\ P$ is the hole untrapping rate given in s^{-1}.
5. As concerns the CB electron capture, we introduce an electron relaxation rate $1/\tau_n$ given in s^{-1} by $1/\tau_n = E_{ct}\ N_t$, so that

$$E_{ct}\ n\ (N_t - n_t) = \frac{n}{\tau_n}\left(1 - \frac{n_t}{N_t}\right). \tag{24}$$

6. We do the same for the VB hole capture by introduction a hole relaxation rate given in s^{-1} by $1/\tau_p = H_{vt}\ N_t$, so that

$$H_{vt}\ p\ n_t = \frac{p}{\tau_p}\ \frac{n_t}{N_t}. \tag{25}$$

Then, the PDE equations are rewritten as

$$\frac{dn}{dt} = G - \frac{n}{\tau_{bb}} + g_n n_t - \frac{n}{\tau_n}\left(1 - \frac{n_t}{N_t}\right), \tag{26}$$

$$\frac{dp}{dt} = -\frac{p}{\tau_{bb}} + G - \frac{p}{\tau_p}\frac{n_t}{N_t} + g_p(N_t - n_t) \tag{27}$$

and

$$\frac{dn_t}{dt} = -g_n n_t + \frac{n}{\tau_n}\left(1 - \frac{n_t}{N_t}\right) + g_p(N_t - n_t) - \frac{p}{\tau_p}\frac{n_t}{N_t}. \tag{28}$$

Depending on the type of laser excitation the three photo-generation rates g_n, g_p and G, which are proportional to the optical power, can be appropriately adjusted [19].

3 Two-level model

It is useful to analyze the GR processes in a simplified two-level model where the TL are absent, which corresponds to a perfect intrinsic semiconductor. This situation can be also used as a

validation model to analyze the interplay between the different characteristic times of the system. In this case, the equation (28) for n_t disappears and equations (26) and (27) become

$$\frac{dn}{dt} = G - \frac{n}{\tau_{bb}} \tag{29}$$

and

$$\frac{dp}{dt} = G - \frac{p}{\tau_{bb}}, \tag{30}$$

where it is trivial that $n(t)$ and $p(t)$ will exhibit the same temporal dynamics determined by the interplay between the generation processes, modeled by the G term, and the recombination processes controlled by the band-to-band recombination time τ_{bb}. This latter, depending on the chosen semiconductor, can vary within a quite large domain of values [22, 23]. In our case, we choose a reasonable value $\tau_{bb} = 1$ μs corresponding to some typical semiconductor as GaAs, InP, InGaAs and amorphous Si [24] but it is evident that, from a physical point of view, what matters is just the comparison between the value of τ_{bb} and the time scale of generation processes, i.e. G. Therefore the model can be easily generalized to other situations where the value of τ_{bb} can be significantly different from 1 μs.

As a first situation, we consider the case of a pulse excitation where the generation rate takes a gaussian form $G = G_0 \exp\left[-\frac{(t-t_0)^2}{2\sigma^2}\right]$ where G_0 represents the maximum of the function, t_0 its center and σ^2 its variance. Indeed, in many practical cases the temporal behavior of a laser pulse is approximated by a gaussian function [25]. Here we choose a value $G_0 = 2 \times 10^{16}$ cm^{-3}s^{-1}. We report in Fig. 4 the behavior of $n(t)$ for different values of σ. We remark that when σ (i.e. approximately the time duration of the pulse) is larger than τ_{bb}, the concentration of photoexcited electrons and holes follow the behavior of $G(t)$ and keep also a gaussian shape reaching a maximum value determined by the stationary solution $n(t) = G\,\tau_{bb} = 2\times10^{10}$ cm^{-3} as shown in Fig. 4(a). However when σ becomes comparable or smaller than τ_{bb} we observe two main modifications: the density of photoexcited electrons and holes does not exhibit a gaussian shape anymore and its maximum value progressively decreases as the duration of the excitation decreases (see Fig. 4(b)).

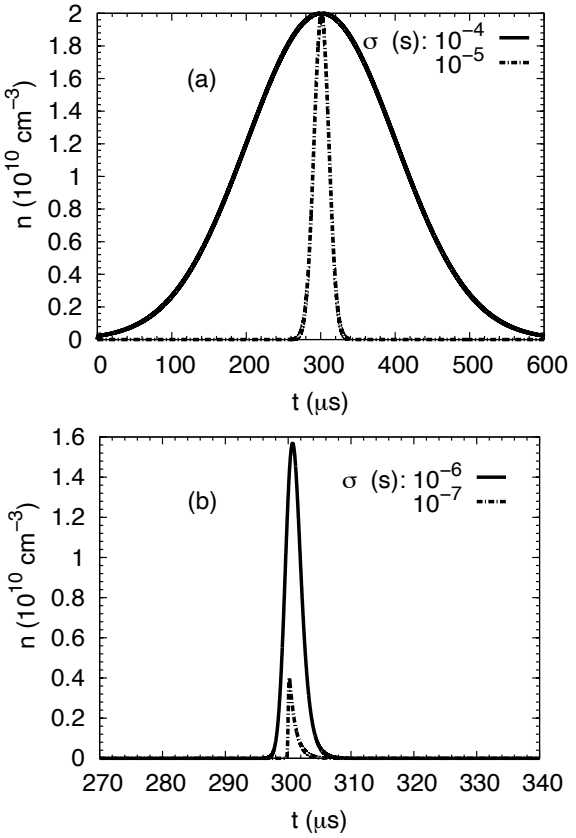

Fig. 4: Electrons concentration $n(t)$ as a function of time in the presence of a gaussian excitation. (a) Standard deviation $\sigma = 10^{-4}$ s and 10^{-5} s. (b) Standard deviation $\sigma = 10^{-6}$ s and 10^{-7} s.

A similar behaviour is obtained if the generation rate is described by a rectangular function of the type $G(t) = G_0\Pi_\theta(t - t_0)$ where t_0 represents the center of the function and θ its duration. The results are shown in Fig. 5 for different values of θ. Indeed, we observe that if the duration of the laser excitation is longer than the band-to-band recombination time the density of electrons and holes keeps a shape similar to $G(t)$ even if the rise and fall parts are not sharp but governed by τ_{bb} as shown in Fig. 5(a). However, when the duration of the pulse θ becomes comparable or smaller than τ_{bb}, the shape of $n(t)$ is progressively modified in a smiliar way as observed in the case of a gaussian perturbation, i.e. the response is no longer rectangular and the maximum value of $n(t)$ decreases with decreasing value of θ (see Fig. 5(b)). It is interesting to analyse the maximum density of

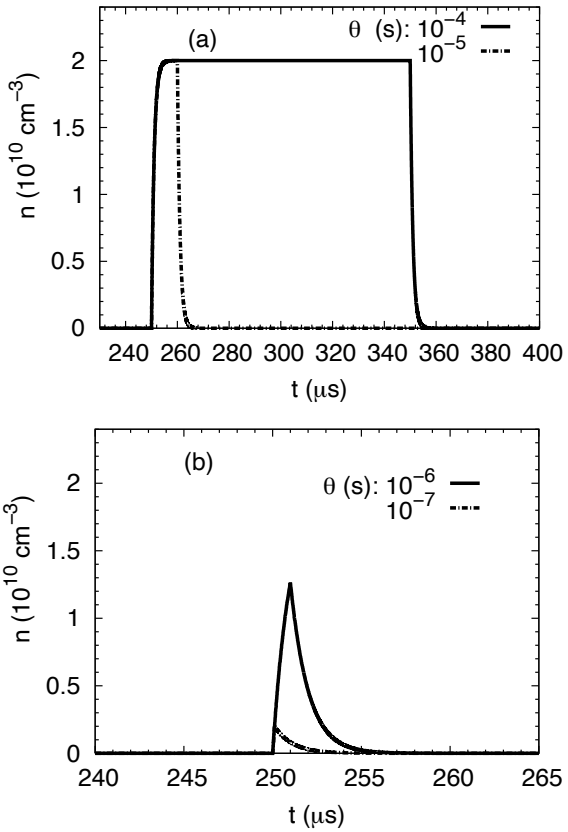

Fig. 5: Electrons concentration $n(t)$ as a function of time in the presence of a square excitation. (a) Duration $\theta = 10^{-4}$ s and 10^{-5} s. (b) Duration $\theta = 10^{-6}$ s and 10^{-7} s.

photoexcited electrons and holes as a function of the pulse duration (i.e. σ for the gaussian case and θ for the rectangular case) as shown in Fig. 6. We remark that, independently of the temporal shape of the excitation, when its characteristic duration becomes smaller than τ_{bb} the photoexcitation is progressively less effective and the maximum concentration of photoexcited carriers is smaller than expected due to the fact that the system cannot reach the stationary conditions.

Another type of excitation can be obtained by superposing two CW lasers with close frequencies thus producing a laser beating where the envelope of the two signals behave as an harmonic function oscillating at the difference frequency [26]. This technique is typically used for frequency down– or up–conversion as, for instance, in the case of CW terahertz generation [27, 28]. Figure 7 reports the

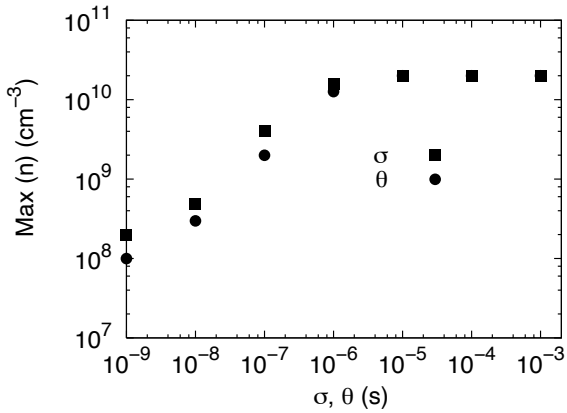

Fig. 6: Maximum values of the electrons concentration $n(t)$ as functions of the standard deviation of a gaussian excitation σ (closed circles) and of the duration of a square excitation θ (closed squares).

temporal behavior of $n(t)$ for two beating frequencies: the former one ($f = 10^7$ Hz) is comparable to the inverse of the band-to-band recombination time ($1/\tau_{bb} = 10^6$ Hz) while the latter one ($f = 10^{12}$ Hz) is much bigger. In all cases, after an initial transient, the time behavior of $n(t)$ is harmonic with an oscillating frequency corresponding to the beating frequency of the lasers. However the amplitude of the oscillations decreases when the beating frequency increases and becomes greater than $1/\tau_{bb}$.

This effect is shown in Fig. 8 which reports the maximum and minimum values of the concentration of photoexcited carriers as functions of the beating frequency: we observe that at increasing beating frequencies the amplitude of the oscillations becomes significantly reduced.

This effect should be taken into account since it can reduce the up-conversion efficiency. One possibility to counteract the effect in the reduction of the amplitude of the harmonic oscillations is to increase the generation rate which, from a practical point of view, means to increase the power of the laser. Therefore in Fig. 9 we have reported the value of G_0 that should be employed to recover the initial values of electrons concentration $n(t)$ which is determined by the stationary condition and equal to $n(t) = 2\times\ 10^{10}$ cm^{-3}.

For very short pulse durations the results shown in Fig. 9 demonstrate that the amplitude of

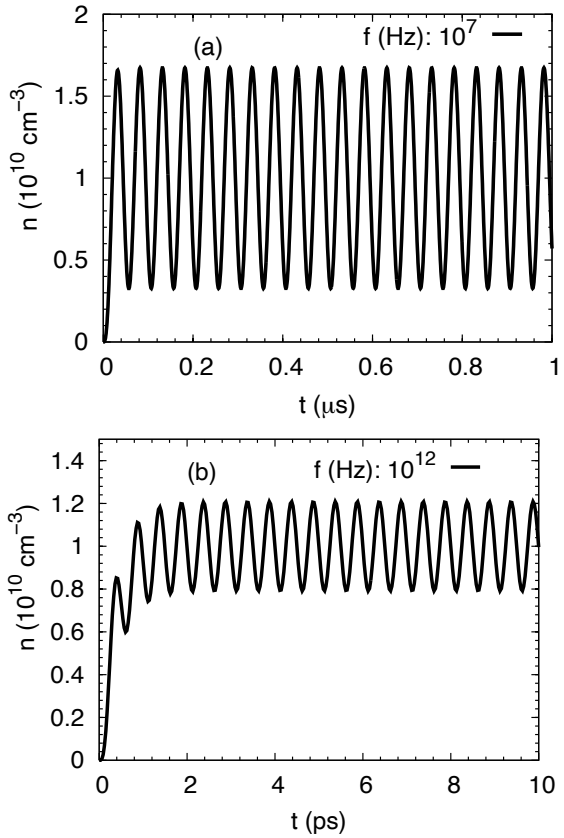

Fig. 7: Electrons concentration $n(t)$ as a function of time in the presence of a harmonic excitation. (a) Frequency $f = 10^7$ Hz. (b) Frequency $f = 10^{12}$ Hz.

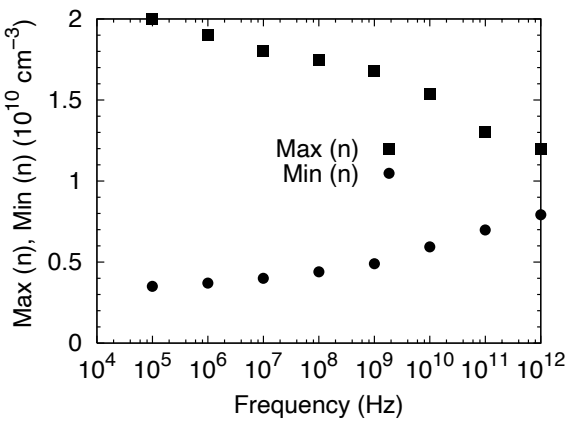

Fig. 8: Maximum values (closed squares) and minimum values (closed circles) of the electrons concentration $n(t)$ as functions of the frequency of a harmonic excitation.

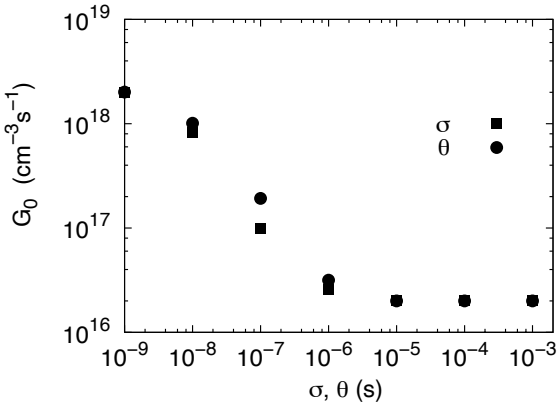

Fig. 9: Value of the amplitude of the excitation G_0 to recover the initial maximum electrons concentrations as function of σ (closed circles) and θ (closed squares).

the laser excitation should be increased of almost two orders of magnitude in order to recover the same concentration of photocarriers.

4 Three-level model

In this section, we consider the GR dynamics in the presence of TL which are supposed to be located in a generic position within the band gap and to act as traps for electrons as well as for holes, as illustrated in Fig. 3. The study of the transitions of electrons and holes through the TL is here presented in two steps: at first we analyze the transient behavior of the different concentrations starting from an initial arbitrary state in the absence of laser excitation, then, in a second time and when the stationary state is achieved, we discuss the effect of the presence of different types of laser excitations.

4.1 Transient behavior in the absence of photoexcitation

For the study of the transient behavior we consider the initial state corresponding to all energy levels empty, i.e. $n(t) = p(t) = n_t(t) = 0$. Before analyzing the results of simulations, it is worthwhile to remark that analytical solutions for the stationary values of the different concentrations can be obtained. Indeed, by solving the system of coupled equations (26),(27) and (28) without

band-to-band generation G, we get the following expressions:

$$n = \frac{g_p\,(N_t - n_t)}{\dfrac{1}{\tau_{bb}} + \dfrac{1}{\tau_p}\dfrac{n_t}{N_t}} \tag{31}$$

and

$$p = \frac{g_n n_t}{\dfrac{1}{\tau_{bb}} + \dfrac{1}{\tau_n}\left(1 - \dfrac{n_t}{N_t}\right)}, \tag{32}$$

where

$$n_t = \frac{-g_p N_t \left(\dfrac{\tau_n}{\tau_{bb}} + 1\right)}{-g_p\left(2 + \dfrac{\tau_n}{\tau_{bb}}\right) - g_n \dfrac{\tau_n}{\tau_{bb}}}, \tag{33}$$

which can be compared to the numerical results.

Figure 10 shows the transient behavior of the different concentrations when the generation rates of electrons and holes are equal. If, in addition to the condition that $g_n = g_p$, both quantities are almost equal to $1/\tau_n = 1/\tau_p$, the time evolutions of electrons and holes concentrations remain nearly the same and exhibit an exponential increasing behavior (see Fig. 10(a)). In this situation only one time scale determines the transient behavior. The decreasing of the untrapping rates $g_n = g_p$ to a value equal to $1/\tau_{bb}$ (i.e. the inverse of the band-to-band recombination time) modifies significantly the transient behavior of $n(t)$ and $p(t)$ which are no longer equal at any time as in the previous case (see Fig. 10(b)). Here, before reaching an equal stationary value, $p(t)$ exhibits an overshoot behavior evidencing the presence of two time scales.

In both cases the stationary value of $n_t(t)$ is equal to $N_t/2$ which indicates that the TL are half occupied and half empty.

It is interesting to study the effects induced by a change in the generation and recombination rates on the different concentrations. In order to keep the analysis sufficiently simple, we keep $\tau_n = \tau_p$ when discussing the effect of a change in the generation rate and $g_n = g_p$ when the recombination rate is varied as shown in Figs. 11(a) and (b), respectively.

On one hand, when the electron generation rate is increased to a value equal to $10g_p = \frac{10}{\tau_{bb}}$,which favors the transitions of electrons from TL to the CB, we observe a quite similar increase of $n(t)$ and $p(t)$. However an increase of g_n is accompanied by a significant decrease of the TL concentration $n_t(t)$ as evidenced in Fig. 11(a) and confirmed by eq. (33). In addition, in this situation, the recombination processes between the band and the TL (given by the case $\tau_p = \tau_n$) are dominant compared to the band-to-band processes (governed by τ_{bb}).

On the other hand, when the electron recombination time is slowed down to a value $\tau_n = 10$ τ_p but keeping equal generation rates ($g_n = g_p$), the transient of $n(t)$ toward its stationary value becomes longer and a more significant difference is observed on the time evolutions of $n(t)$ and $p(t)$ as reported on Fig. 11(b). Moreover, the TL become

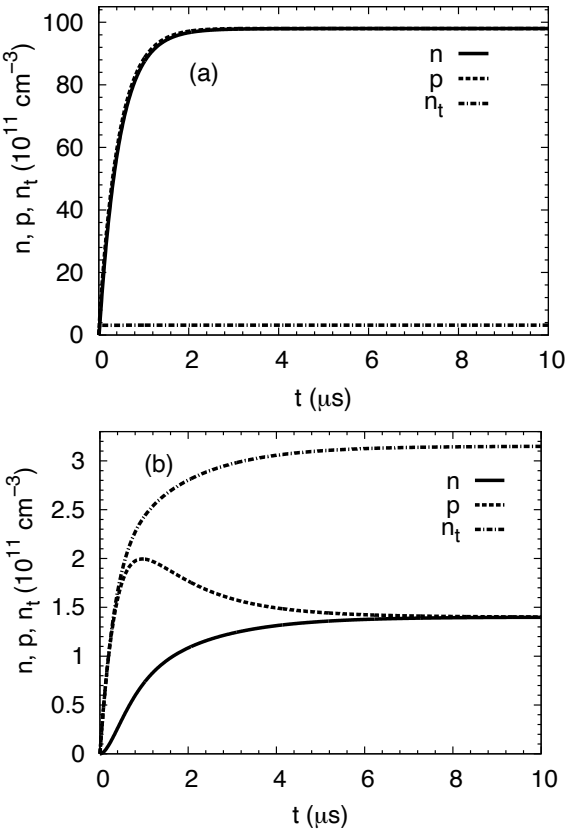

Fig. 10: Electrons $n(t)$, holes $p(t)$ and traps $n_t(t)$ concentrations as functions of time in the absence of photoexcitation with $\tau_{bb} = 10^{-6}$ s, $\tau_n = \tau_p = 4{\times}10^{-7}$ s and $N_t = n_0 = 6.3{\times}10^{11}$ cm^{-3}. We take (a) $g_n = g_p = 7{\times}10^{7}$ cm^{-3}s^{-1} and (b) $g_n = g_p = 10^{6}$ cm^{-3}s^{-1}.

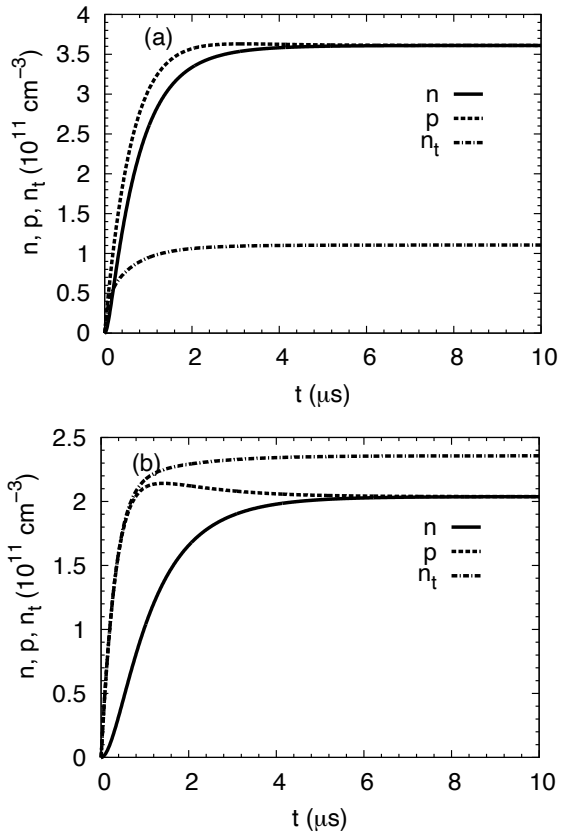

Fig. 11: Electrons $n(t)$, holes $p(t)$ and traps $n_t(t)$ concentrations calculated for different electrons generation rates g_n and recombination times τ_n with $\tau_{bb} = 10^{-6}$ s, $\tau_p = 4 \times 10^{-7}$ s, $g_p = 10^6$ cm^{-3}s^{-1} and $N_t = n_0$. We take (a) $g_n = 10g_p$ with $\tau_n = \tau_p$ and (b) $\tau_n = 10\tau_p$ with $g_n = g_p$.

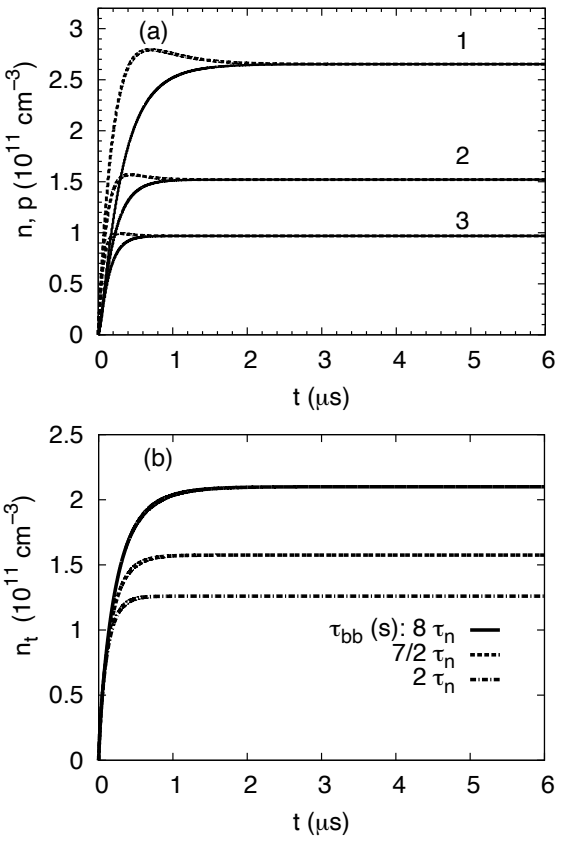

Fig. 12: (a) Electrons $n(t)$ (continuous lines) and holes $p(t)$ (dotted lines) concentrations, (b) traps $n_t(t)$ concentration as functions of time calculated for $\tau_{bb} = 8\tau_n$ (curves labeled 1), $\tau_{bb} = 7/2\tau_n$ (curves labeled 2), $\tau_{bb} = 2\tau_n$ (curves labeled 3). The other parameters are $\tau_n = 4 \times 10^{-7}$ s, $g_n = 1/\tau_n = 10g_p$, $g_p = 1/\tau_p$ and $N_t = n_0$.

more filled by electrons (i.e. the stationary value of $n_t(t)$ increases) while band-to-band processes do not have a significant influence.

Indeed, the effect of band-to-band recombination on the time evolution of the different concentrations is analyzed in Fig. 12 where calculation are performed for the case $g_n = 1/\tau_n = 10g_p$ and $g_p = 1/\tau_p$.

We remark that in this case eqs. (31), (32) and (33) are simplified to:

$$n = \frac{\gamma N_t}{\frac{\tau_n}{\tau_{bb}} + (1-\gamma)}, \tag{34}$$

$$p = \frac{N_t(1-\gamma)}{\frac{\tau_p}{\tau_{bb}} + \gamma} \tag{35}$$

and

$$n_t = \gamma N_t, \tag{36}$$

where $\gamma = \dfrac{\tau_n + \tau_{bb}}{11\tau_n + 2\tau_{bb}}$

The progressive decreasing of τ_{bb} by the values $8\tau_n$, $\frac{7}{2}\tau_n$ and $2\tau_n$ leads to smaller values of the TL filling equal to $N_t/3$, $N_t/4$ and $N_t/5$, respectively, as can be easily shown through eq. (36) where $\gamma = \frac{1}{3}$, $\frac{1}{4}$ and $\frac{1}{5}$. Indeed when the band-to-band recombination becomes faster, there is a weaker probability that TL are occupied thus leading to the decrease of $n_t(t)$ shown in Fig. 12(b).

In parallel, the concentration of electrons and holes as well as the duration of the transient increase when the band-to-band recombination processes are slow, as shown in Fig. 12(a). In contrast, the recombination processes from CB, VB and TL are much less important for smaller values of τ_{bb}: this leads also to smaller stationary values of electrons and holes concentrations

4.2 Gaussian photoexcitation

After reching their stationary values, we analyze here the effect of a pulse band-to-band photoexcitation having a gaussian form of the same type as studied in section 3. Moreover, since this previous study has evidenced that there is no significant physical difference in the responses to a square with respect to a gaussian excitation, we have here limited our analysis only to the second case.

In Fig. 13 we present the time evolutions of the three concentrations $n(t)$, $p(t)$ and $n_t(t)$ resulting from a gaussian photoexcitation of different durations (i.e. different standard deviations) superimposed to the respective stationary values. Again, to simplify the analysis, we have considered only two situations: the former one corresponding to $g_n = g_p$ and the latter one corresponding to $g_n = 10g_p$.

The stationary photocarriers concentrations (electron n and hole p) increase from 1.4×10^{11} cm^{-3} to 3.6×10^{11} cm^{-3} when the electron generation rate increases from $g_n = g_p$ to $g_n = 10g_p$ (see Fig. 13(a)), however their time evolutions remain similar in both cases. Indeed, as long as the duration of the pulse is comparable or longer than the recombination times (and inverse generation rates), the time behaviors of $n(t)$ and $p(t)$ follow the shape of the photoexcitation impulse.

When the duration of the pulse becomes shorter, we observe a progressive decreasing of the maximum values of $n(t)$ and $p(t)$ and significant deviations from the gaussian shapes which become strongly asymmetric (see curves labelled 2 and 3 in Fig. 13(a)). As a result, the spectral content of the photoconduction will be significantly modified.

In parallel, high values for the TL occupation can be observed in the case of $g_n = 10g_p$ (see Fig. 13(b)). while it keeps a constant value for the case $g_n = g_p$, which means that no additional filling of TL is observed in the second case. For this reason the curves of $n_t(t)$ are reported

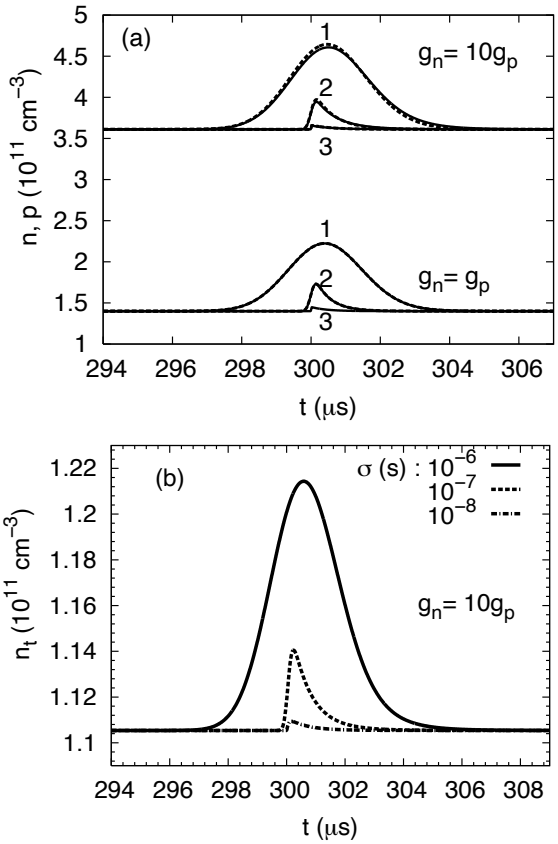

Fig. 13: (a) Electrons $n(t)$ (continuous line) and holes $p(t)$ (dashed lines) concentrations as functions of time calculated for $g_n = g_p$ and $g_n = 10g_p$. Curves labeled 1, 2 and 3 correspond to standard deviations of the gaussian photoexcitation $\sigma = 10^{-6}$ s, 10^{-7} s and 10^{-8} s, respectively. (b) Traps $n_t(t)$ concentrations as functions of time calculated for $g_n = 10g_p$ and the reported standard deviations. The other parameters are $\tau_{bb} = 10^{-6}$ s, $\tau_n = \tau_p = 4 \times 10^{-7}$ s, $g_p = 10^6$ cm^{-3}s^{-1} and $N_t = n_0$.

in Fig. 13(b) only when $g_n = 10g_p$. In summary, for high electron generation rate ($g_n = 10g_p$) and longer photoexcitation time ($\sigma = 10^{-6}$ s), the generation processes of photocarriers in CB, VB and TL are favored more than the recombination process toward de TL, and a sharp pic in n_t concentration is obtained.

Figure 14 illustrates the time evolutions of $n(t)$, $p(t)$ and $n_t(t)$ for the same standard deviations as in Fig. 13 but calculated for two different situations: equal recombination times $\tau_n = \tau_p$

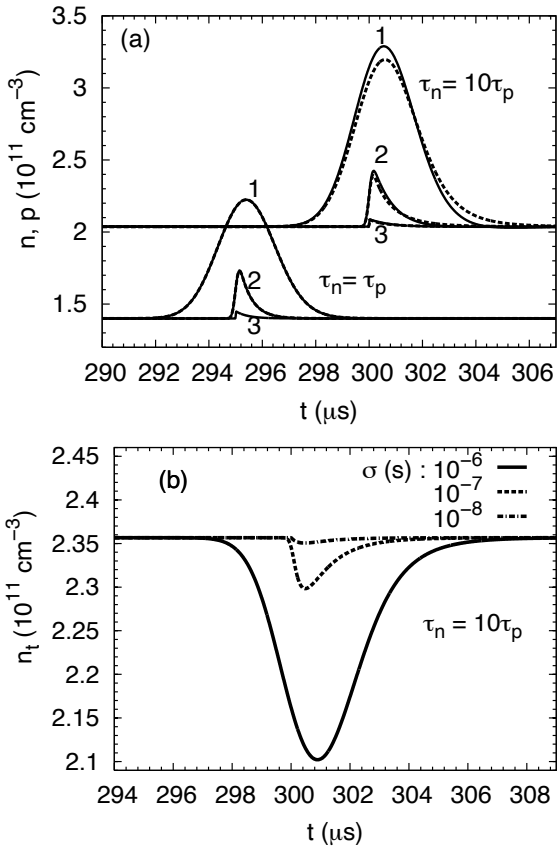

Fig. 14: (a) Electrons $n(t)$ (continuous line) and holes $p(t)$ (dashed lines) concentrations as functions of time calculated for $\tau_n = \tau_p$ and $\tau_n = 10\tau_p$. Curves labeled 1, 2 and 3 correspond to standard deviations of the gaussian photoexcitation $\sigma = 10^{-6}$ s, 10^{-7} s and 10^{-8} s, respectively. (b) Traps $n_t(t)$ concentrations as functions of time calculated for $\tau_n = 10\tau_p$ and the reported standard deviations. The other parameters are $\tau_{bb} = 10^{-6}$ s, $\tau_p = 4{\times}10^{-7}$ s, $g_n = g_p = 10^6$ cm^{-3}s^{-1} and $N_t = n_0$.

and faster electron recombination time $\tau_n = 10\tau_p$ but, in both cases, keeping equal generation rates $g_n = g_p$. To avoid superimposition of the curves, the central time of the gaussian photoexcitation has been shifted in Fig. 14(a).

Analogously to the results shown in Fig. 13, the stationary values of $n(t)$ and $p(t)$ depend on the values of the recombination times and they are actually equal to 2.1×10^{11} cm^{-3} (for $\tau_n = \tau_p$) and 1.4×10^{11} cm^{-3} (for $\tau_n = 10\tau_p$).

Despite a slight difference in the time evolutions of $n(t)$ and $p(t)$, which has been already evidenced in the study of the transient behavior (see for instance Fig. 11(b)), the results obtained by varying the recombination time are qualitatively similar to those obtained by varying the generation rates previously shown in Fig. 13.

The main difference concerns the behavior of the occupied traps concentration $n_t(t)$. Indeed, while for the case $\tau_n = \tau_p$ no change in $n_t(t)$ is observed (not reported in Fig. 14(b)), an increase of the electron recombination time to a value $\tau_n = 10\tau_p$ favors a decrease of the population of electrons on the TL because they spend more time in the CB. As a consequence, $n_t(t)$ exhibits the reversed behavior shown in Fig. 14(b) evidencing that a larger effect is obtained for a longer duration of the gaussian photoexcitation (see the case $\sigma = 10^{-6}$ s in Fig. 14(b)). In contrast, a faster pulse ($\sigma = 10^{-8}$ s) leads to an almost constant value of n_t because almost no trasition to the TL is observed.

4.3 Harmonic photoexcitation

In this section we consider a harmonic excitation of two CW lasers oscillating at the beating frequency f applied to the three-level bulk semiconductor where the stationary condition is already achieved. This harmonic excitation is assumed to pump the electrons from the VB to the CB. This band-to-band generation is modelled by introducing the generation rate $G = G_0\,(\sin(2\pi f))^2$ in eqs. (26) and (27).

The effect of electron generation rate $g_n = 10g_p$ and electron recombination time $\tau_n = 10\tau_p$ on the temporal behavior of electron $n(t)$, hole $p(t)$ and traps $n_t(t)$ is reported in Fig. 15 (a) and (b), respectively.

A harmonic response corresponding to the beating frequency of the laser photoexcitation is observed in the reponse of all concentrations. In addition, the amplitude of the oscillations is found to depend, on the one side, on the excitation frequency and, on the other side, on the values of the generation rates and recombination times.

To get a better physical insight into these processes we have focused the attention on the maximum and minimum values of the concentrations oscillations. The effect on the amplitude of the concentrations oscillations of a progressive

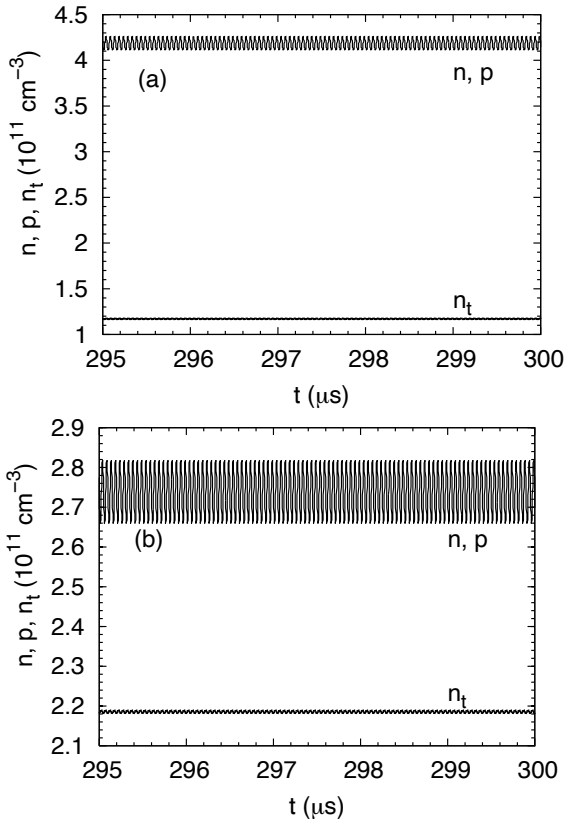

Fig. 15: Electrons $n(t)$, holes $p(t)$ and traps $n_t(t)$ concentrations as functions of time in the presence of a harmonic excitation of frequency $f = 10^7$ Hz. (a) Electron generation rate $g_n = 10g_p$ and (b) Electron recombination time $\tau_n = 10\tau_p$. The other parameters are $\tau_{bb} = 10^{-6}$ s, $\tau_p = 4 \times 10^{-7}$ s, $g_p = 10^6$ cm^{-3}s^{-1}, $G_0 = 2 \times 10^{16}$ cm^{-3}s^{-1} and $N_t = n_0$.

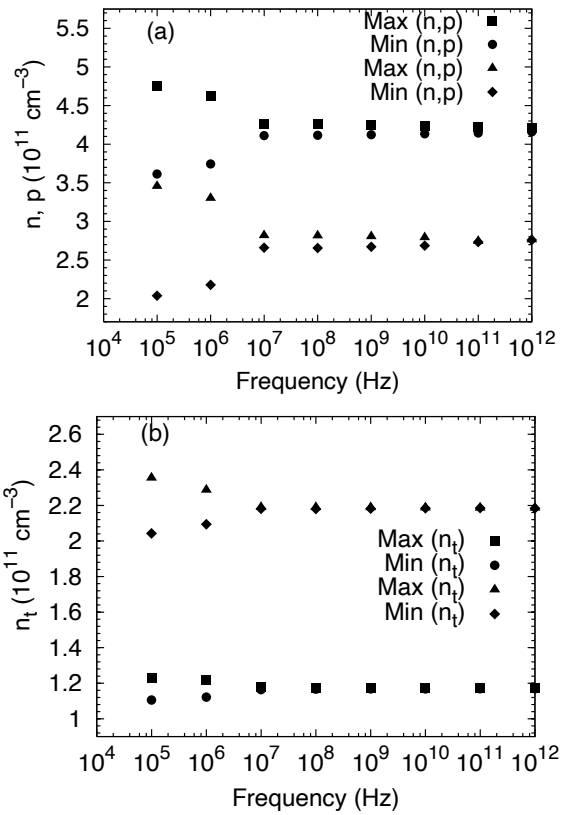

Fig. 16: Maximum and minimum values of (a) electrons $n(t)$ and holes $p(t)$ concentrations and (b) traps n_t concentration as functions of the frequency under harmonic excitation calculated for $g_n = 10g_p$ (squares and circles) and for $\tau_n = 10\tau_p$ (triangles and diamonds). The other parameters are $\tau_{bb} = 10^{-6}$ s, $\tau_p = 4 \times 10^{-7}$ s, $g_p = 10^6$ cm^{-3}s^{-1} and $N_t = n_0$.

increase of the frequency of the photoexcitation from $f = 10^4$ Hz (i.e. a value much smaller than the different generation rates and inverse recombination times) to $f = 10^{12}$ Hz (i.e. a value much greater than the different generation rates and inverse recombination times) is analyzed in Fig. 16. As a general trend we observe that, in the low frequency region, the amplitude of the oscillations of all concentrations is great, which is a consequence of the fact that $n(t)$, $p(t)$ and $n_t(t)$ follow the time behavior of $G(t)$ as if the system was near to quasi-stationary conditions. Moreover a slightly higher amplitude of the oscillations is found in the electrons and holes concentrations for an increased electrons recombination time (triangles and diamonds in Fig. 16(a)) than for an increased electrons generation rate (squares and circles in Fig. 16(a)). This effect is reversed if the oscillations in the traps concentration is observed as reported in Fig. 16(b). When the frequency of the photoexcitation becomes comparable to the shortest characteristic time of the system (either a recombination time or an inverse generation rate), the amplitude of all the concentrations oscillations tend to progressively disappear since the system is no longer able to follow to excitation signal.

5 Conclusion

In this paper, we have studied the semiconductor photoconductivity dynamics under pulse and harmonic laser excitations in the frameworks of two-level and three-level models.

The analysis is based on the numerical solution of the system of partial differential equations for the concentrations of electrons, holes and occupied trap levels considering all the physical processes responsible for the transitions of photocarriers between the bands and the traps level. The presence of an electric field and diffusion phenomena are neglected and could be topics for futures studies.

In the first simplified situation (two-level model), the calculations consider the generation-recombination processes between the valence and conduction bands with different scenarios of laser excitation. The pulse temporal behavior of a laser was approximated by gaussian and rectangular functions where the influence of the time duration of the pulse on the electrons and holes concentrations has been investigated. For the continuous wave excitation the temporal behavior of the concentrations follows the harmonic excitation while its amplitude has been found to depend on the beating frequency.

In the second situation (three-level model), the dynamics of electrons, holes and occupied traps concentrations are discussed in two steps. In the former one, we considered the trasient behavior starting from empty bands and traps levels in the absence of any laser excitation and we studied the influence of the generation and recombination characteristic times.

In the latter one, we have considered the presence of pulse or harmonic laser excitations while the influence of their duration and frequency on the stationary behaviors of electrons, holes and occupied traps concentrations have been analysed with respect to the intrinsic characteristic times of the system.

These results pave the way for a better understanding of photoconductivity dynamics in semiconductors under optical regime and could be useful to predict the performances of present and future photoconductive devices and systems.

References

[1] Bube R.: Photoelectronic Properties of Semiconductors, Cambridge Univ. Press, 1992

[2] E. Castro-Camus and M. Alfaro: Photoconductive devices for terahertz pulsed spectroscopy. Photon. Res,**4,** Number 3 (2016). https://doi.org/10.1364/PRJ.4.000A36.

[3] Jingyi Yu, Lingyan Xu, Binbin Zhang and Wanqi Jie: Photocarrier transport dynamics in lifetime and relaxation regimes of semiconductors containing traps. Materials Research Express,**7,** Number 1 (2019). https://doi.org/10.1088/2053-1591/ab57b9

[4] Tonouchi M.: Cutting-edge terahertz technology. Nature Photon **1,** 97-105 (2007). https://doi.org/10.1038/nphoton.2007.3

[5] Dhillon S.S., Vitiello M.S., Linfield E.H., et al.: The 2017 terahertz science and technology roadmap. J. Phys. D: Appl. Phys. **50** 043001 (2017). https://doi.org/10.1088/1361-6463/50/4/043001

[6] Ishibashi T., et al.: Uni-Traveling-Carrier Photodiodes. OSA Trends in Optics and Photonics Series **13,** paper UC3 (1997). https://doi.org/10.1364/UEO.1997.UC3

[7] Ishibashi T., Ito H.: Uni-traveling-carrier photodiodes. J. Appl. Phys. **127**, 031101 (2020). https://doi.org/10.1063/1.5128444

[8] Nagatsuma T., Ducournau G., Renaud C.C.: Advances in terahertz communications accelerated by photonics. Nature Photon **10,** 371-379 (2016). https://doi.org/10.1038/nphoton.2016.65

[9] Ducournau G., et al.: THz communications using Photonics and Electronic devices: the Race to Data-Rate. J Infrared Milli Terahz Waves **36**, 198-220 (2015). https://doi.org/10.1007/s10762-014-0112-x

[10] Saeedkia D., Mansour R.R., Safavi-Naeini S.: Analysis and Design of a Continuous-Wave Terahertz Photoconductive Photomixer Array Source. IEEE Trans. Antennas Propag. **53,** 4044-4050 (2005). https://doi.org/10.1109/TAP.2005.859909

[11] Rouvalis E., et al.: High-speed photodiodes for InP-based photonic integrated circuits. Opt. Express **20,** 9172-9177 (2012). https://doi.org/10.1364/OE.20.009172

[12] Berry C.W., et al.: Significant performance enhancement in photoconductive terahertz

optoelectronics by incorporating plasmonic contact electrodes. Nat Commun **4,** 1622 (2013). https://doi.org/10.1038/ncomms2638

[13] Yardimci N. T. and Jarrahi M.: Nanostructure-Enhanced Photoconductive Terahertz Emission and Detection. Small **14**, 1802437 (2018). https://doi.org/10.1002/smll.201802437

[14] Neshat M., et al.: A Global Approach for Modeling and Analysis of Edge-Coupled Traveling-Wave Terahertz Photoconductive Sources. IEEE Trans. Microw. Theory Tech. **58,** 1952-1966 (2010). https://doi.org/10.1109/TMTT.2010.2050379

[15] Ameen D.B. and Tait G.B.: Convolution-Based Global Simulation Technique for Millimeter-Wave Photodetector and Photomixer Circuits. IEEE Trans. Microw. Theory Tech. **50,** 2253-2258 (2002). https://doi.org/10.1109/TMTT.2002.803436

[16] Stepanov A. G., Hebling J. and Kuhl J.: Generation, tuning, and shaping of narrow-band, picoseconds THz pulses by two-beam excitation. Optics Express **12**, 4650-4658 (2004). https://doi.org/10.1364/OPEX.12.004650

[17] Khabiri M., Neshat M. and Safavi-Naeini S.: Hybrid Computational Simulation and Study of Continuous Wave Terahertz Photomixers. IEEE Trans Terahertz Sci Technol **2**, 605-616 (2012). https://doi.org/10.1109/TTHZ.2012.2213596

[18] Pasqualini D., Neto A., Wyss, R.A.: Distributed sources on coplanar waveguides: Application to photomixers for THz local oscillators. Microwave Opt Technol Lett **33,** 430-435 (2002). https://doi.org/10.1002/mop.10342

[19] Sze S. M. and Ng K. K.: Physics of Semiconductor Devices 3rd ed. Hokoben, N.J: Wiley-Interscience (2007). https://www.doi.org/10.1002/0470068329

[20] Nêmec H., et al.: Ultrafast carrier dynamics in Br^++-bombarded InP studied by time-resolved terahertz spectroscopy. Phys. Rev. **B78,** 235206 (2008). https://link.aps.org/doi/10.1103/PhysRevB.78.235206

[21] Fekete L. et al.: Ultrafast carrier response of Br^+-irradiated In0.53Ga0.47As excited at telecommunication wavelengths. J. of Appl. Phys. **111,** 093721 (2012). https://doi.org/10.1063/1.4709441

[22] Laurentis De M. and Irace A.: Optical Measurement Techniques of Recombination Lifetime Based on the Free Carriers Absorption Effect. Journal of Solid State Phys. 1-19 (2014). DOI:10.1155/2014/291469

[23] Cuevas A. and Macdonald D.: Measuring and Interpreting the Lifetime of Silicon Wafers. Sol. Energy. **76,** 255-262 (2004). DOI:10.1016/j.solener.2003.07.033

[24] Arunas Krotkus.: Semiconductors for terahertz photonics applications. Journal of Physics D, Applied Physics, IOP Publishing. **27,** 273001 (2010). DOI:10.1088/0022-3727/43/27/273001

[25] Sharma A. and Kourakis I.: Spatial evolution of a q-Gaussian laser beam inrelativistic plasma. Laser and Particle Beams. **28,** 479-489 (2010). doi:10.1017/S0263034610000479

[26] HR Telle, Guenter Steinmeyer, Dunlop AE. and Stenger J.: Carrier-envelope offset phase control:A novel concept for absolute optical frequency measurement and ultrashort pulse generation. Appl. Phys. B. **69(4),** 327-332 (1999). doi:10.1007/s003400050813

[27] Namje Kim, Jaeheon Shin, Eundeok Sim, Chul Wook Lee, Dae-Su Yee, Min Yong Jeon, Yudong Jang and Kyung Hyun Park.: Monolithic dual-mode distributed feedback semiconductor laser for tunable continuous-wave terahertz generation. Optics Express. **17,** 13851-13859 (2009). https://doi.org/10.1364/OE.17.013851

[28] Alexei Moussatov, Bernard Castagnede and Vitalyi Gusev.: Frequency up-conversion and frequency down-conversion of acoustic waves in damaged materials. Physics Letters A. **301(3),** 281-290 (2002). doi:10.1016/S0375-9601(02)00974-X